Journal of Inflammation Research

Dovepress
Taylor & Francis Group

Open Access Full Text Article

ORIGINAL RESEARCH

# Mechanistic Exploration of Shenling Baizhu Powder in Treating Irinotecan-Associated Diarrhea: A Study Based on Network Pharmacology and Experimental Validation

Meng Liu[1], Ying Xiong[2], Jun Yuan[3], Qi Jin[3], Jin-Cheng Zhang[2], Run-Jia Shi[2], Zhi-Qiang Cheng[1]

[1]Oncology Department of Integrated Traditional Chinese and Western Medicine, China-Japan Friendship Hospital, Beijing, People's Republic of China; [2]Department of Radiation Oncology, China-Japan Friendship Hospital, Beijing, People's Republic of China; [3]Graduate School, Beijing University of Chinese Medicine, Beijing, People's Republic of China

Correspondence: Zhi-Qiang Cheng, Oncology Department of Integrated Traditional Chinese and Western Medicine, China-Japan Friendship Hospital, Beijing, People's Republic of China, Email zhiqiangcheng@163.com



**Objective:** Irinotecan-associated diarrhea (IAD) is a severe adverse effect that limits its clinical utility in cancer therapy. Shenling Baizhu Powder (SLBZP), a traditional Chinese herbal formula, has shown potential in alleviating chemotherapy-induced gastrointestinal toxicity, but its mechanism against IAD remains unclear. This study integrated network pharmacology and experimental validation to systematically explore the therapeutic mechanisms of SLBZP in IAD.

**Methods:** Network pharmacology approaches were employed to identify bioactive components of SLBZP and their targets using the TCMSP database, while IAD-related targets were retrieved from Genecards. Protein-protein interaction (PPI) analysis and KEGG pathway enrichment were performed to pinpoint core targets and signaling pathways. For in vivo validation, an IAD rat model was established via tail vein injection of irinotecan (150 mg/kg), with SLBZP intervention and Gegen Qinlian Decoction (GGQLD) as a positive control. In vitro, LPS-stimulated NCM460 cells were treated with SLBZP water extract. Mechanistic evaluations were performed using molecular biology techniques, including ELISA, qPCR, and Western blotting, to validate the underlying mechanisms.

**Results:** Network pharmacology analysis revealed that SLBZP exerted therapeutic effects against IAD by closely interacting with multiple inflammatory-related targets and pathways. In vivo studies demonstrated that SLBZP significantly ameliorated diarrhea severity, improved histopathological manifestations in intestinal tissues, and suppressed the expression of key inflammatory cytokines (TNF-α, IL-6, and IL-1β). Mechanistically, SLBZP inhibited the aberrant activation of inflammatory signaling pathways, including PI3K/AKT, MAPK, and NF-κB. Consistent findings were observed in vitro, where SLBZP water extract attenuated inflammatory responses in LPS-stimulated NCM460 cells.

**Conclusion:** Integrated network pharmacology analysis and experimental validation demonstrate that SLBZP alleviates IAD primarily by suppressing intestinal inflammatory responses, providing mechanistic evidence to support its clinical application in managing chemotherapy-induced intestinal toxicity.

**Keywords:** Shenling Baizhu Powder, irinotecan-associated diarrhea, network pharmacology, inflammatory response

## Introduction

Irinotecan (CPT-11), a potent topoisomerase I inhibitor, has served as a cornerstone chemotherapeutic agent in colorectal cancer management since receiving clinical approval in the late 1980s.[1] However, irinotecan-associated diarrhea (IAD), a dose-limiting toxicity, significantly impairs patients' treatment tolerance and quality of life.[2] The pathogenesis of IAD is complex, involving multiple pathophysiological processes such as intestinal mucosal injury, exacerbated inflammatory responses, gut microbiota dysbiosis, and inhibition of metabolic enzyme UGT1A1 activity.[3–6] While loperamide persists as the cornerstone antidiarrheal agent in current clinical practice, such symptomatic approaches demonstrate variable

Received: 23 April 2025
Accepted: 23 September 2025
Published: 3 October 2025

interpatient efficacy and neglect the fundamental pathophysiology of irinotecan-induced dysbiotic gut microenvironment.[7] Thus, exploring therapeutic strategies with multi-target regulatory properties and high safety profiles holds critical clinical significance.

Traditional Chinese medicine (TCM) has demonstrated unique advantages in alleviating chemotherapy-induced toxicities.[8] An accumulating number of recent studies have suggested that medicinal herbs and their derived phytocompounds may be effective complementary treatments for chemotherapy-induced diarrhea.[9–12] Shenling Baizhu Powder (SLBZP), a classical formula for "strengthening the spleen and replenishing qi", has long been used clinically to treat diarrhea caused by spleen deficiency and dampness accumulation.[13] Its herbal components are rich in polysaccharides, saponins, and flavonoids, which exhibit potential anti-inflammatory, immunomodulatory, and gut barrier-protective activities. Recent studies suggest that SLBZP may ameliorate chemotherapy-induced gastrointestinal toxicity through synergistic multi-component, multi-target, and multi-pathway mechanisms.[14,15] However, its specific molecular mechanisms in mitigating IAD remain systematically unelucidated.

Network pharmacology, through systematic integration of component screening, target prediction, and pathway enrichment analysis, serves as a powerful methodological tool for elucidating the intricate polypharmacological networks underlying TCM formulas.[16–20] This study employs network pharmacology combined with experiments validation to unravel the key components, core targets, and signaling pathways through which SLBZP modulates IAD. The findings aim to provide scientific evidence for the modernized application of TCM in managing chemotherapy-associated diarrhea and to establish a novel methodological paradigm for mechanistic research on classical herbal formulas.

# Materials and Methods

## Network Pharmacology Prediction

### Acquisition and Collection of Key Targets

The Traditional Chinese Medicine Systems Pharmacology Database and Analysis Platform (TCMSP, https://www.tcmsp-e.com/#/database)[21] was utilized to retrieve the components of SLBZP (composed of Ren Shen, Fu Ling, Bai Zhu, Sha Ren, Gan Cao, Shan Yao, Jie Geng, Yi Yi Ren, Bai Bian Dou and Lian Zi Rou). Components with oral bioavailability (OB) ≥ 30% and drug-likeness (DL) ≥ 0.18 were defined as key components.[22,23] Gene targets corresponding to these key components were extracted from TCMSP, and standardized using the UniProt database (https://www.uniprot.org/) to ensure compliance with HUGO gene nomenclature guidelines.[24] The resulting targets were designated as SLBZP-related targets.

The GeneCards database (https://www.genecards.org/)[25] was queried using the keywords "Irinotecan" and "Diarrhea" to obtain Irinotecan-related targets and Diarrhea-related targets, respectively. The bioinformatics online platform (http://www.bioinformatics.com.cn/) was employed to generate Venn diagrams for visualizing overlaps among SLBZP-related targets, Irinotecan-related targets, and Diarrhea-related targets. The intersection of all three groups was defined as the therapeutic targets of Shenling Baizhu San for Irinotecan-induced diarrhea. A regulatory network encompassing SLBZP, its constituent herbs, key components, and targets was constructed. Visualization was performed using Cytoscape 3.9.1 to elucidate the multi-component, multi-target therapeutic relationships.

### Prediction of Treatment-Related Mechanisms

The therapeutic targets of Shenling Baizhu San for Irinotecan-induced diarrhea were imported into the STRING database (https://string-db.org/)[26] to construct a protein-protein interaction (PPI) network. Parameters were set as follows: organism "Homo sapiens", interaction confidence threshold ≥ 0.700, and disconnected nodes were excluded to retain high-confidence interactions. The resulting PPI network was exported in TSV format and visualized using Cytoscape 3.9.1. Nodes were arranged with layout algorithms to optimize network topology. Core targets were identified by calculating the degree of connectivity (number of edges per node), and the top 20 targets with the highest connectivity were selected for subsequent analysis.

Based on the R 4.2.1 platform (www.r-project.org/), the clusterProfiler package (version 4.6.2) was utilized to perform Kyoto Encyclopedia of Genes and Genomes (KEGG) pathway enrichment analysis on the core targets. The org.Hs.eg.db database provided gene annotation for Homo sapiens. Pathways associated with human diseases or basal

metabolism (eg, metabolic pathways, cancer-related pathways) were excluded. The top 20 significantly enriched signaling pathways were selected to establish a "target-pathway" regulatory network, which was visualized using Cytoscape to elucidate potential therapeutic mechanisms.

## Experimental Validation

The reagents and antibodies used in the experiments are detailed in the Supplementary Material.

### Animal Model Establishment

A total of 36 male 4-week-old specific pathogen-free (SPF) Sprague-Dawley (SD) rats were purchased from Beijing Speyford Biotechnology Co., Ltd. The sample size of animal experiment was estimated through the degrees of freedom in analysis of variance.[27] All experimental procedures involving rats were approved by the Animal Ethics Committee of the China-Japan Friendship Hospital (Approval No. ZRYHYY21-22-08-06) and were conducted in strict compliance with the 3R principles (Replacement, Reduction, Refinement) to ensure ethical animal welfare standards. The housing conditions for rats comply with the "Laboratory Animal-Requirements of Environment and Housing Facilities" (GB 14925–2010, National Laboratory Animal Standardization Technical Committee of China). After a 1-week acclimatization period, the 36 rats were randomly divided into four groups (n=9 per group) using a random number table: blank control group, model group, SLBZP group, and Gegen Qinlian Decoction (GGQLD). Starting on days 4 and 5 of the experiment, the model group, SLBZP group, and GGQLD group received 150 mg/kg irinotecan via tail vein injection based on body weight to establish an irinotecan-induced diarrhea model, while the blank control group was administered an equivalent volume of normal saline.

### Drug Formulation and Intervention Protocols in Animal Studies

SLBZP was composed of Ren Shen (15g), Fu Ling (15g), Bai Zhu (15g), Shan Yao (15g), Bai Bian Dou (12g), Lian Zi Rou (9g), Yi Yi Ren (9g), Sha Ren (6g), Jie Geng (6g) and Gan Cao (9g), totaling 111 g of crude herbs. The clinical dosage for adults was one formula daily, decocted in water. Assuming an adult body weight of 70 kg, the human equivalent dose of SLBZP was calculated as 1.586 g/kg (crude drug dry weight/adult body weight). Based on the human-to-rat body surface area conversion factor,[28] the rat dose was adjusted to 10 g/kg (crude drug dry weight/rat body weight). One formula of SLBZP was concentrated to 111 mL (yielding a concentration of 1 g/mL, crude drug dry weight/herbal solution volume), sterilized, and stored at 4°C. The administered dose for rats was 10 mL/kg (herbal solution volume/rat body weight).

GGQLD contained Ge Gen (24 g), Huang Qin (9 g), Huang Lian (9 g), Gan Cao (6 g), totaling 48 g. The clinical human-to-rat was calculated as 0.686 g/kg (crude drug dry weight/adult body weight). Using the same conversion method, the rat dose was 4.32 g/kg (crude drug dry weight/rat body weight). One dose of GGQLD was concentrated to 111 mL (concentration: 0.432 g/mL, crude drug dry weight/herbal solution volume), sterilized, and stored at 4°C. The administered dose for rats was 10 mL/kg (herbal solution volume/rat body weight).

In the animal experiment, from day 1 to day 9, all groups received daily intragastric administration at 8:00 AM, with the normal control group and model group administered distilled water at a volume of 10 mL/kg body weight, while the SLBZP group and GGQLD group received 10 mL/kg of the prepared SLBZP and GGQLD, respectively, based on their body weights.

### Body Weight and Diarrhea Assessment

Body weight was measured daily throughout the experimental period. Starting 24 hours after the initial irinotecan administration, diarrhea severity in rats was assessed daily using the Akinobu-Kurita scoring method, with detailed criteria provided in Supplementary table 1.[29]

### Sample Processing Protocols in Animal Studies

Following anesthesia with isoflurane, the abdominal area of rats was shaved and the skin was surgically incised using a scalpel. Blood samples were collected from the abdominal aorta using sterile blood collection needles and vacuum tubes, followed by 30-minute incubation at room temperature. Subsequently, centrifugation was performed (4°C,

3000 rpm, 15 min), and the obtained serum was stored at −80°C. The jejunal tissues were dissected, thoroughly rinsed with PBS, and divided into two portions: one fixed in 4% paraformaldehyde for subsequent pathological examination, and the other snap-frozen in liquid nitrogen and stored at −80°C for molecular biology analyses.

### Histopathological Examination of Jejunal Tissue

The jejunal tissue samples washed with PBS were fixed in 4% paraformaldehyde solution for 24 hours, followed by dehydration through a graded ethanol series (70%, 80%, 90%, 95%, and 100%) with each concentration maintained for 30 minutes. After dehydration, the samples were cleared by immersion in xylene twice (30 minutes each). The dehydrated tissues were subsequently embedded in paraffin and sectioned into 3 μm-thick slices using a microtome. The sections were flattened on the surface of 45°C warm water and mounted onto glass slides. The paraffin-embedded sections were dewaxed with xylene and rehydrated through a descending ethanol gradient. Hematoxylin and eosin (HE) staining was performed according to the manufacturer's protocol, followed by sealing with neutral balsam.[30] The prepared sections were scanned using a panoramic scanner to evaluate histopathological alterations in jejunal tissues.

### Cell Culture

The NCM460 cell lines were purchased from Shanghai Cellverse Co., Ltd. Complete RPMI 1640 medium was prepared by supplementing the base medium with 10% fetal bovine serum (FBS) and 1% penicillin-streptomycin, followed by pre-warming in a 37°C water bath. Cryopreserved NCM460 cells were retrieved from liquid nitrogen and immediately thawed in a 37°C water bath with gentle agitation until fully liquefied. The thawed cell suspension was mixed with pre-warmed RPMI 1640 complete medium and centrifuged (4°C, 800 rpm, 5 minutes). The supernatant was discarded, and the cell pellet was resuspended in fresh RPMI 1640 complete medium. Cells were then transferred to a humidified incubator (37°C, 5% $CO_2$) for expansion. Subsequent experiments were conducted when cells reached the logarithmic growth phase.

### Preparation of Drugs for in vitro Cell-Based Assays

One dose of SLBZP was decocted in 1.1 L of water for 1 hour and filtered through sterile gauze to collect the decoction. This decoction process was repeated twice, and the three filtrates were combined. The pooled filtrate was concentrated to 500 mL under reduced pressure using a rotary evaporator. The concentrate was stored at 4°C for 12 hours, followed by centrifugation (4°C, 10,000×g, 15 minutes) to collect the supernatant. The supernatant was heated to boiling, and absolute ethanol was added under continuous stirring until the ethanol content reached 70% (v/v). After equilibration to room temperature, the mixture was centrifuged (4°C, 10,000 × g, 15 minutes) to remove precipitates. The ethanol-containing supernatant was further concentrated under reduced pressure and lyophilized using a vacuum freeze-dryer. The final lyophilized powder was weighed for yield calculation. The lyophilized SLBZP was reconstituted in PBS and filtered through a 0.22 μm membrane for cell treatment.

### Rational Design of Drug Concentration Gradients for in vitro Studies

NCM460 cells in the logarithmic growth phase were detached via trypsinization and resuspended in complete RPMI 1640 medium to prepare a cell suspension at a density of 50,000 cells/mL. A 100 μL aliquot of the cell suspension was seeded into each well of a 96-well plate. After cell adherence, the medium was replaced with complete RPMI 1640 medium containing varying concentrations of SLBZP. Following 48 hours of treatment, the medium was aspirated, and cells were washed twice with PBS. Subsequently, 100 μL of RPMI 1640 basal medium was added to each well, and cells were incubated for an additional 4 hours. CCK-8 reagent was then introduced, and the plate was incubated for 1 hour. Optical density (OD) was measured at 450 nm using a microplate reader. Five replicate wells were set up for each intervention concentration, with the mean OD value used as the final readout. A preliminary range-finding experiment was conducted prior to the formal assay to determine appropriate concentration ranges. Cell viability under varying SLBZP concentrations was calculated based on OD values using the formula: Viability (%) = 100×(OD of treated sample-OD of medium)/(OD of control sample-OD of medium).

The maximum concentration demonstrating no significant cytotoxicity was designated as the high-dose group, with medium- and low-dose groups set at 1/2 and 1/4 of this concentration, respectively.

### Malondialdehyde (MDA) and Superoxide Dismutase (SOD) Assays

MDA and SOD levels were determined via chemical assays. Following reagent preparation as per the protocol, OD values were recorded using a microplate reader, and serum concentrations were calculated using pre-established standard curves.

### ELISA Assay

A 20 mg aliquot of jejunal tissue was homogenized in 1 mL PBS and centrifuged at 10,000 rpm for 10 minutes at 4°C. The resulting supernatant was collected as the sample for ELISA analysis. Prior to the assay, the ELISA kit was removed from refrigeration and equilibrated to room temperature for 30 minutes. Wash buffer, biotinylated antibody working solution, and enzyme conjugate working solution were prepared according to the manufacturer's instructions, while standard solutions were serially diluted. During the assay, 100 μL of samples or diluted standards were added to each well of an antibody-precoated microplate, followed by 50 μL of biotinylated antibody working solution. The plate was sealed with adhesive film and incubated at room temperature for 120 minutes. After discarding the liquid, wells were washed four times with wash buffer and blotted dry on absorbent paper. Subsequently, 100 μL of enzyme conjugate working solution was added to each well, and the plate was resealed and incubated for an additional 30 minutes at room temperature. Following repeated washing and drying, 100 μL of chromogenic substrate (TMB) was added to each well, and the plate was incubated in the dark at room temperature for 15 minutes. The reaction was terminated by adding 100 μL of stop solution per well. Optical density (OD) at 450 nm was immediately measured using a microplate reader. A standard curve was generated by plotting OD values against known standard concentrations with CurveExpert software, and sample protein concentrations were calculated through interpolation.[31]

### Total RNA Extraction and qRT-PCR Analysis

Total RNA was extracted from tissue samples using the TRIzol method. Briefly, 20 mg of tissue was placed in a pre-chilled 1.5 mL grinding tube containing 1 mL TRIzol reagent and grinding beads. In the animal study, the tissue was homogenized thoroughly in a tissue homogenizer, followed by centrifugation (4°C, 10,000 × g, 10 minutes) to collect the supernatant.

A volume of 550 μL isopropanol was added to the supernatant, gently inverted for 15 seconds, and centrifuged (4°C, 10,000 × g, 10 minutes) to pellet RNA. The supernatant was discarded, and 100 μL chloroform substitute was added to the pellet. After thorough mixing and incubation for 3 minutes, the mixture was centrifuged (4°C, 10,000 × g, 10 minutes), and the supernatant was removed. The RNA pellet was washed twice with 75% ethanol, air-dried at room temperature for 3 minutes, and dissolved in 15 μL DEPC-treated water.[32] RNA concentration and purity were measured using a spectrophotometer.

For reverse transcription, 1 μg RNA was mixed with reagents from a reverse transcription kit in an RNase-free microcentrifuge tube according to the manufacturer's instructions. The reaction mixture was gently pipetted to homogeneity, incubated at 50°C for 15 minutes for cDNA synthesis, and terminated by heating at 85°C for 5 seconds. Quantitative real-time PCR (qRT-PCR) was performed using cDNA, primers (sequences listed in Supplementary table 2), and SYBR Green Real-time PCR Master Mix. Reaction mixtures were prepared following the manufacturer's protocol, and thermal cycling parameters were set as specified. CT values were recorded for each sample. Target gene expression levels were normalized to β-actin or GAPDH, and relative mRNA expression was calculated using the $2^{-\Delta\Delta Ct}$ method.[33]

### Western Blot

The RIPA lysis working solution was prepared by mixing RIPA lysis buffer with protease inhibitors and phosphatase inhibitors. In the animal study, 20 mg of jejunal tissue was weighed and homogenized in 250 μL of RIPA lysis buffer using a glass homogenizer on ice. The homogenate was centrifuged (4°C, 10,000 × g, 10 min), and the supernatant was collected for downstream analyses. For the cell experiments, after treatment, cells cultured in 6-well plates were washed twice with PBS, and 250 μL of RIPA lysis buffer was added. The cells were lysed on ice for 30 min, followed by centrifugation (4°C, 10,000 × g, 10 min) to obtain the supernatant.

The protein concentration of the collected samples was quantified using the Bicinchoninic Acid Assay (BCA), and the concentrations were normalized across samples using RIPA lysis buffer. Protein samples were mixed with 5× Loading

Buffer at a 4:1 ratio, boiled for 10 min, and centrifuged (4°C, 10,000 × g, 10 min). The resulting supernatant was used for subsequent electrophoresis.

10% SDS-PAGE gels were prepared according to the manufacturer's protocol. Protein markers and samples were loaded into the gel lanes, and electrophoresis was performed until the bromophenol blue dye migrated to the bottom of the gel. The SDS-PAGE gel was separated from the glass plates, and PVDF membranes were activated with methanol. A transfer stack consisting of sponge pads, filter paper, SDS-PAGE gel, PVDF membrane, filter paper, and sponge pads was assembled. Proteins were transferred from the gel to the PVDF membrane via electrophoretic transfer.

Following transfer, the PVDF membrane was washed with TBST and blocked with 5% skim milk in TBST for 1 h at room temperature on a shaker. The membrane was incubated with diluted primary antibody at 4°C overnight, followed by five 5-min washes with TBST. Subsequently, a diluted secondary antibody was added and incubated for 1.5 h at room temperature, followed by another five 5-min TBST washes. An ECL working solution was prepared by mixing reagents A and B, and the solution was evenly applied to the PVDF membrane. Chemiluminescent signals were visualized using a fully automated imaging system, and the acquired images were quantitatively analyzed using ImageJ software.[34]

## Data Analysis

Statistical analyses were conducted with SPSS (IBM, USA). Continuous data are presented as mean ± standard deviation (SD). For comparisons between two groups, Student's *t*-test was applied only if both groups met the assumptions of normality (assessed by Shapiro–Wilk test) and homogeneity of variances (assessed by Levene's test). Otherwise, the non-parametric Mann–Whitney *U*-test was used. A p-value $< 0.05$ was considered to indicate a statistically significant difference.

# Results

## Key Targets of SLBZP in the Treatment of IAD

Through screening the TCMSP database, a total of 495 active components from SLBZP were initially identified. Among these, 172 components met the screening criteria of oral bioavailability (OB) ≥30% and drug-likeness (DL) ≥0.18, which were defined as the bioactive components of SLBZP. These 172 bioactive components corresponded to 219 potential therapeutic targets. Retrieval from the Genecards database revealed 935 targets associated with irinotecan and 8,406 targets related to diarrhea. Intersection analysis of these three datasets yielded 92 common targets potentially involved in SLBZP's therapeutic effects against IAD. Subsequently, a multidimensional regulatory network was constructed to visualize the "SLBZP - Herbal Medicine - Bioactive Components - Targets - Disease" relationships, which was graphically represented using Cytoscape software (Figure 1).

## Prediction of the Mechanism of SLBZP in the Treatment of IAD

PPI network analysis of the therapeutic targets of SLBZP for IAD revealed that 89 targets participated in the network construction, comprising 592 interaction edges. The visualized PPI network is shown in Figure 2A. The top 20 targets ranked by the number of interactions included IL6, MYC, STAT3, BCL2, TNF, CTNNB1, IL1B, HIF1A, PTGS2, RELA, BCL2L1, CCND1, MMP9, CASP9, PARP1, CXCL8, EGF, MAPK1, ALB, and CASP8 (Figure 2B). For the KEGG pathway enrichment analysis of the therapeutic targets, 154 signaling pathways were identified. After excluding pathways related to human diseases and metabolism, 74 pathways remained. The top 15 enriched pathways were the PI3K-Akt signaling pathway, MAPK signaling pathway, cellular senescence, IL-17 signaling pathway, apoptosis, HIF-1 signaling pathway, C-type lectin receptor signaling pathway, Th17 cell differentiation, TNF signaling pathway, NOD-like receptor signaling pathway, Toll-like receptor signaling pathway, p53 signaling pathway, NF-kappa B signaling pathway, FoxO signaling pathway, and apoptosis - multiple species (Figure 3A). A total of 55 targets were associated with these pathways, and the top 10 genes ranked by relevance to the pathways were RELA, MAPK1, CHUK, MAPK10, IL-6, MAPK14, CASP8, IL-1β, NFKBIA, and TNF (Figure 3B).

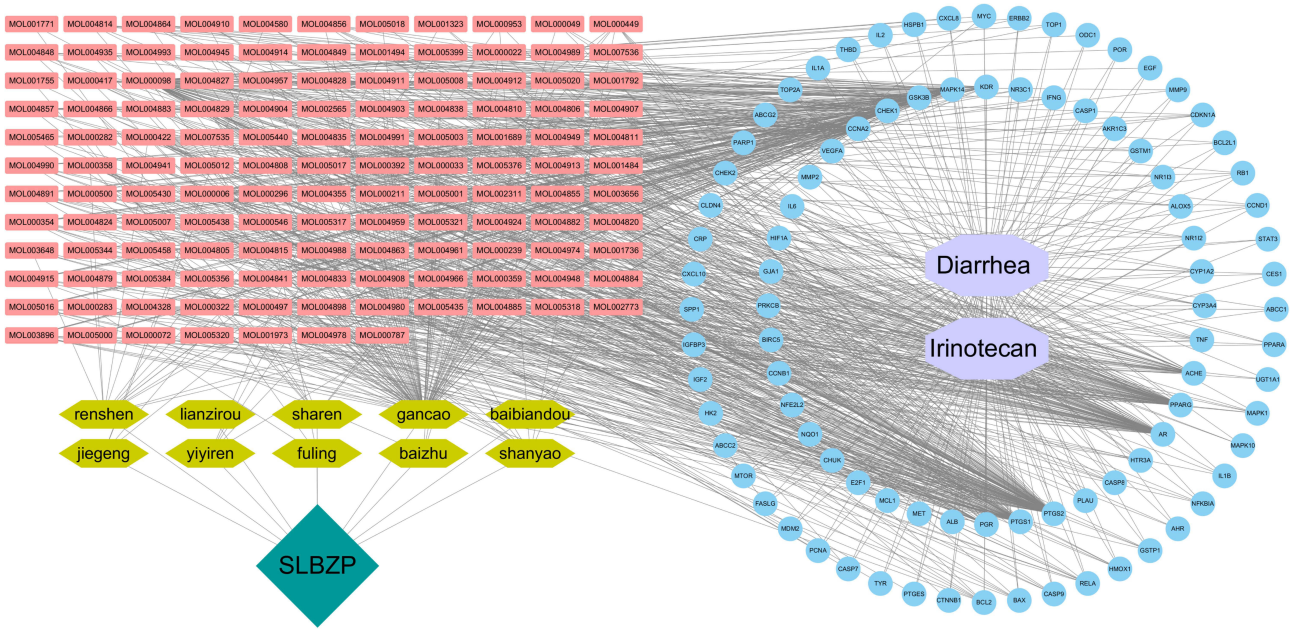


**Figure 1** Regulatory network of "Shenling Baizhu Powder (SLBZP) - Herbal Medicine - Bioactive Components - Targets - Disease".

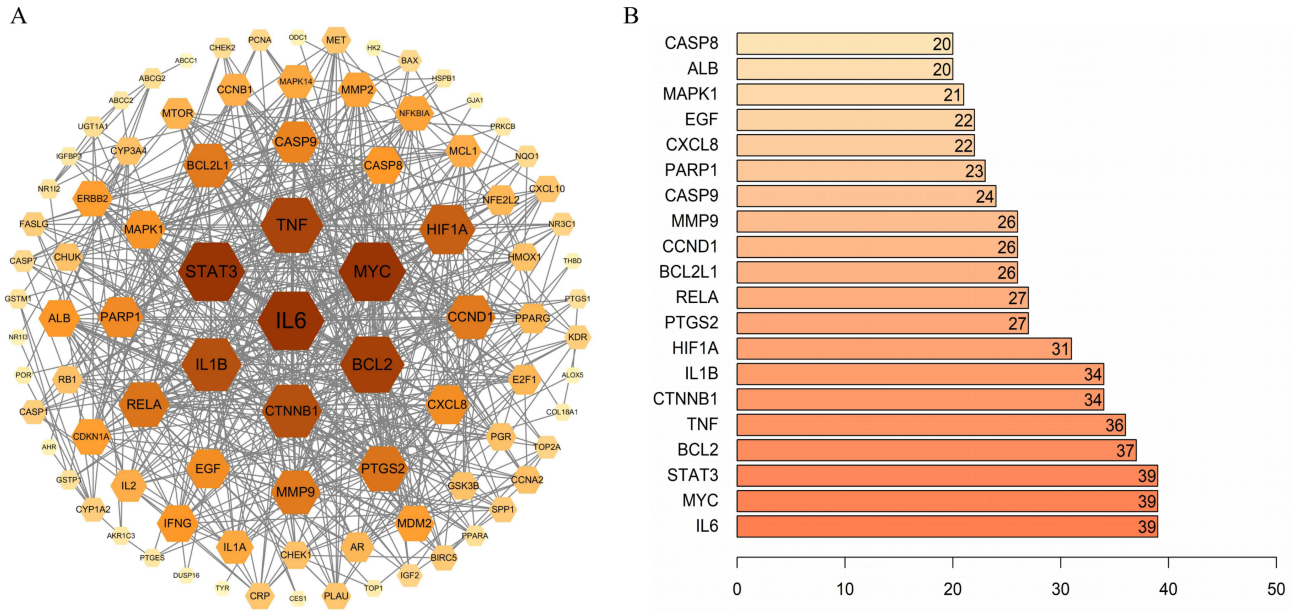


**Figure 2** (**A**) Visualized protein-protein interaction (PPI) network; (**B**) Top 20 targets ranked by connectivity in the PPI network.

## Effects of SLBZP on Body Weight and Diarrhea Severity in a Rat Model of IAD

Following tail vein injection of irinotecan, rats exhibited a progressive decline in daily body weight gain rate, with diarrhea severity assessment commencing on day 5 of the experiment. Notably, both SLBZP and the positive control GGQLD demonstrated therapeutic effects, as evidenced by partial restoration of body weight growth rate (Figure 4A) and attenuation of diarrhea severity (Figure 4B).

## Effects of SLBZP on Intestinal Pathology in a Rat Model of IAD

Histopathological examination of the jejunum via hematoxylin and eosin (H&E) staining demonstrated distinct morphological features across experimental groups. In the blank control group (Figure 5A), the intestinal mucosa exhibited a well-organized structure, characterized by orderly arranged villi and intact crypts with clear architectural boundaries. In contrast,


https://doi.org/10.2147/JIR.S536184

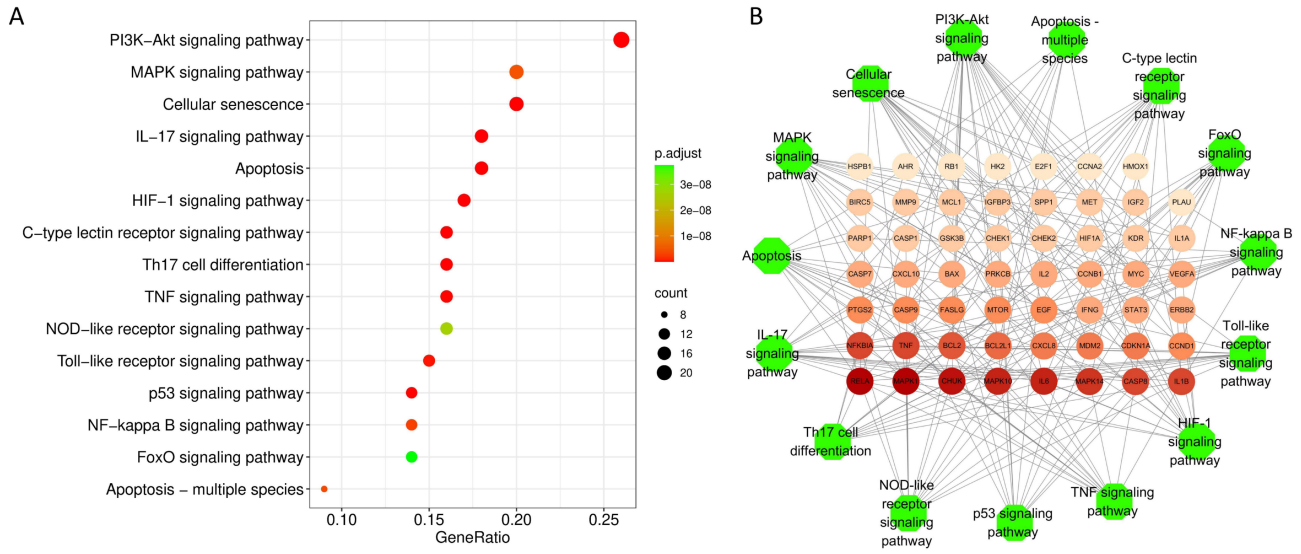


**Figure 3** (**A**) Top 15 enriched signaling pathways from KEGG analysis. (**B**) Visualization of targets associated with the top 15 signaling pathways.

the model group (Figure 5B) displayed severe mucosal injury, manifesting as sparse and fragmented villi, disorganized crypts with structural discontinuity, and disrupted epithelial integrity, accompanied by haphazardly aligned epithelial cells, thereby validating the successful induction of irinotecan-associated diarrhea. Compared to the model group, both the Shenling Baizhu Powder-treated group (Figure 5C) and the GGQLD-treated group (Figure 5D) showed marked amelioration of intestinal pathology, including preserved epithelial continuity, reduced villus fragmentation, and restoration of crypt-villus morphological regularity, indicative of therapeutic efficacy in mitigating mucosal damage.

## Effects of SLBZP on Serum MDA and SOD Levels in a Rat Model of IAD

The levels of oxidative stress-related markers MDA and SOD in serum were measured across all rat groups. The experimental results showed that the oxidative damage marker MDA was significantly increased after the establishment of the IAD model (Figure 6A), while the antioxidant enzyme SOD was markedly decreased in the model group (Figure 6B). Both SLBZP and the positive control drug GGQLD partially reversed these changes to varying degrees (Figure 6A and B).

## Effects of SLBZP on Pro-Inflammatory Cytokines in Intestinal Tissues of a Rat Model of IAD

qPCR and ELISA analyses revealed significantly elevated mRNA (Figure 7A–C) and protein expression levels (Figure 7D–F) of IL-6, IL-1β, and TNF-α in jejunal tissues following IAD induction. Both SLBZP and GGQLD interventions demonstrated marked suppression of these pro-inflammatory cytokine expressions at transcriptional and translational levels (Figure 7A–F).

## Effects of SLBZP on Inflammatory Pathways in Intestinal Tissues of a Rat Model with IAD

Western blot analysis was performed to assess the expression and phosphorylation levels of key proteins (AKT, p38 MAPK, and NF-κB p65) in the PI3K/AKT, MAPK, and NF-κB signaling pathways. The results demonstrated that while total protein expression of AKT, p38 MAPK, and NF-κB p65 remained unchanged following IAD modeling, their phosphorylation levels were markedly increased (Figure 8A). Both SLBZP and GGQLD interventions demonstrated significant inhibitory effects on the phosphorylation of these proteins, suggesting their suppressive roles in counteracting the aberrant activation of PI3K/AKT, MAPK, and NF-κB signaling pathways induced by IAD (Figure 8B–D).

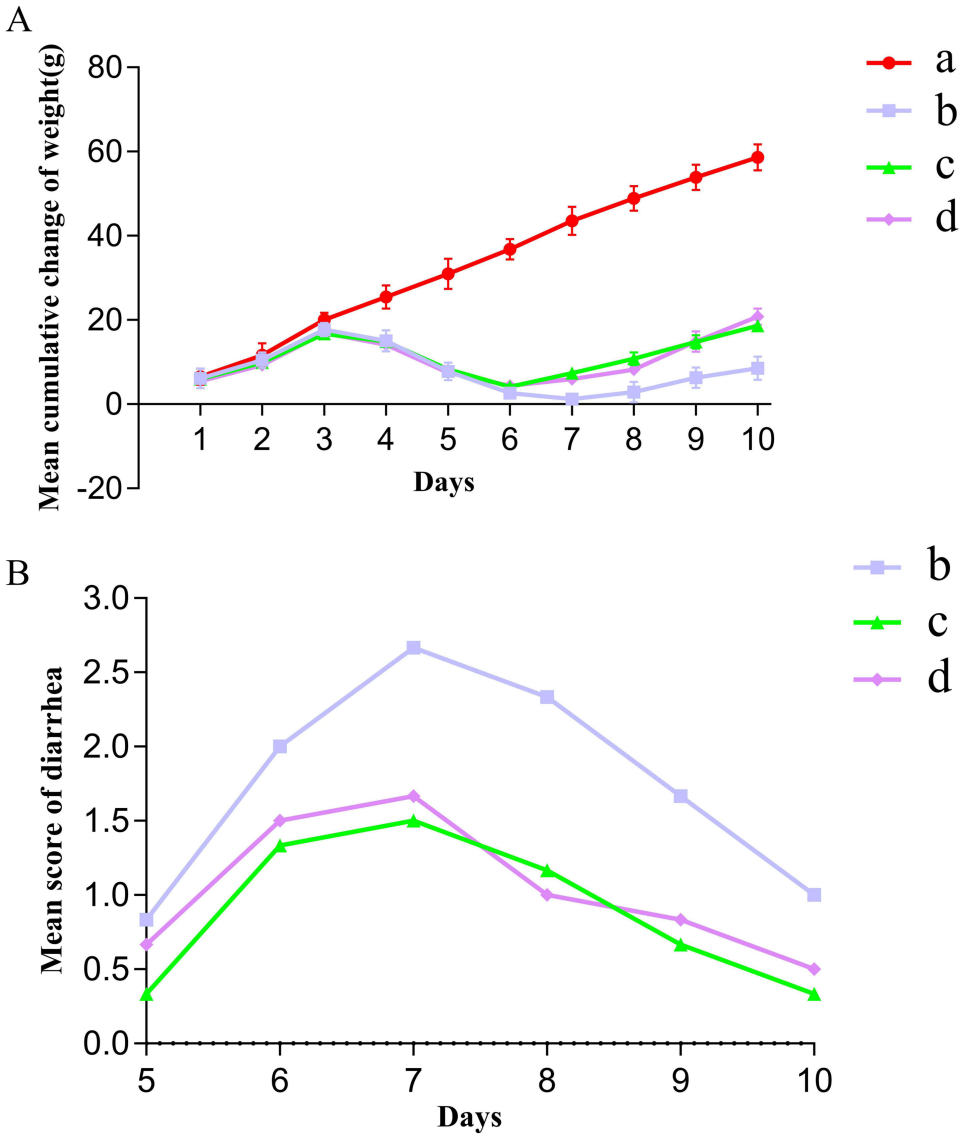


**Figure 4** (**A**) Daily body weight gain rate in rats. (**B**) Diarrhea severity scores. a: Blank control group; b: Model group; c: SLBZP group; d: Gegen Qinlian Decoction (GGQLD) group.

## Optimization of SLBZP Concentration for Cell Intervention via CCK-8 Assay

NCM460 cells were treated with SLBZP aqueous extract at varying concentrations. The results demonstrated that low-concentration SLBZP aqueous extract promoted cell proliferation, whereas inhibitory effect on proliferation was observed when the concentration exceeded 240 mg/L (Figure 9). Based on these findings, subsequent experiments utilized 220 mg/L as the high-dose intervention concentration, 110 mg/L as the medium-dose, and 55 mg/L as the low-dose intervention concentration.

## Effects of SLBZP on Pro-Inflammatory Cytokines in LPS-Stimulated NCM460 Cells

To further investigate the anti-inflammatory effects of SLBZP in vitro, an inflammatory model was established by stimulating NCM460 human colonic epithelial cells with 100 ng/mL LPS. Cells were subsequently treated with SLBZP extract at low (55 mg/L), medium (110 mg/L), and high concentrations (220 mg/L). After 24 hours of intervention, qPCR and ELISA analyses demonstrated that LPS stimulation significantly increased the mRNA and protein expression levels

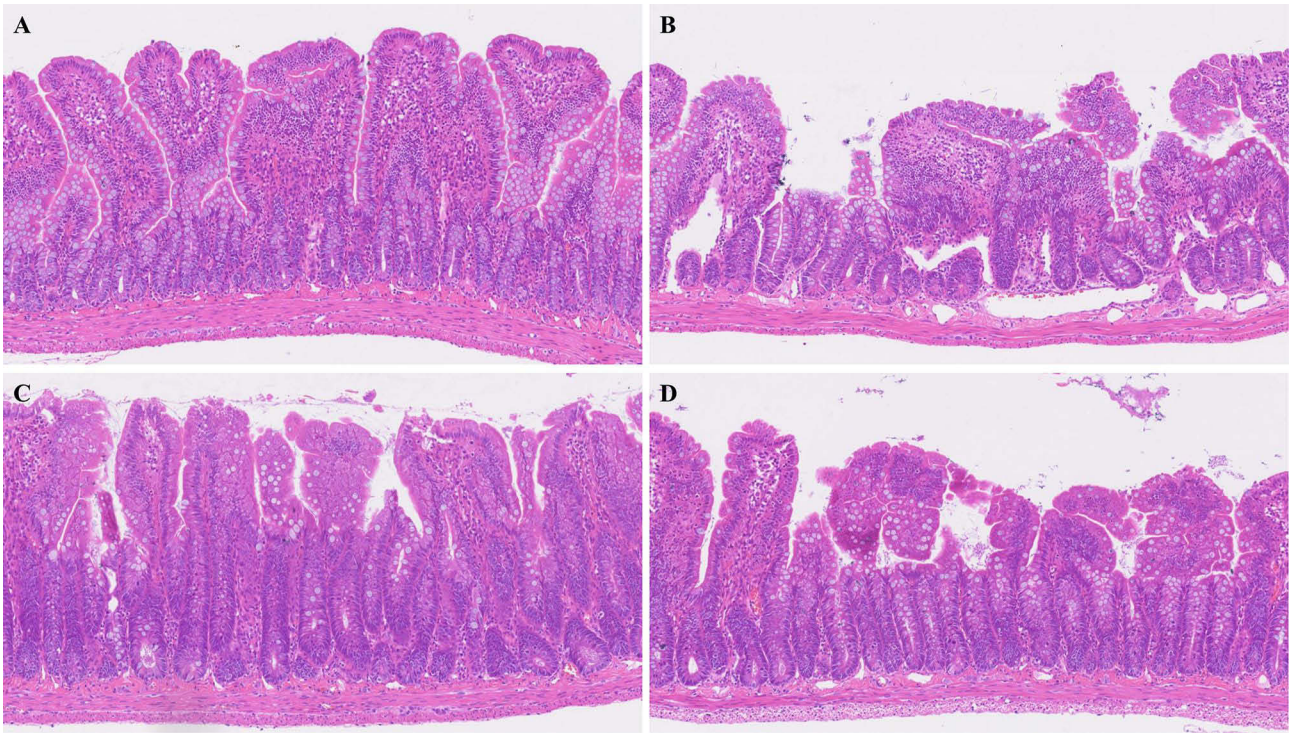


**Figure 5** Histopathological manifestations of intestinal tissues across experimental groups. (**A**) Blank control group; (**B**) Model group; (**C**) SLBZP group; (**D**) GGQLD group.

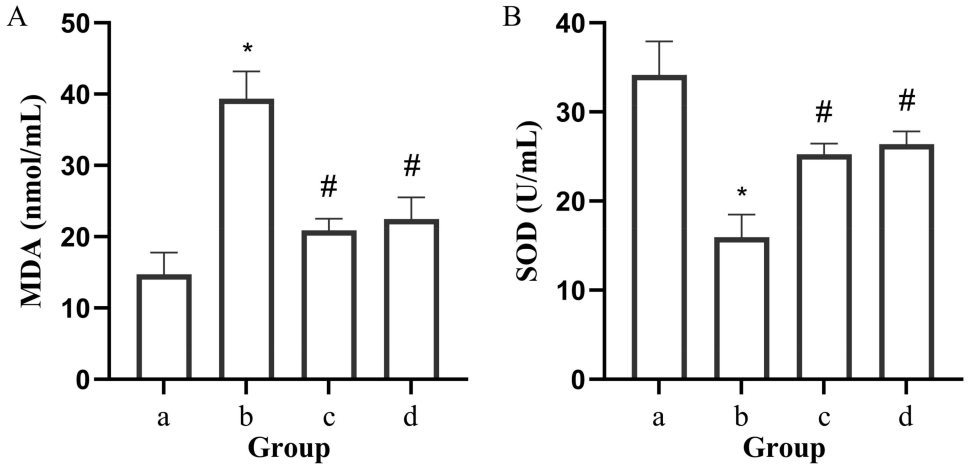


**Figure 6** (**A**) Serum Malondialdehyde (MDA) levels in different groups of rats (n=6). (**B**) Serum Superoxide Dismutase (SOD) levels in different groups of rats (n=6). a: Blank control group; b: Model group; c: SLBZP group; d: GGQLD group. *p<0.05 vs.Blank control group; #p<0.05 vs Model group.

of IL-6, IL-1β, and TNF-α (Figure 10A–F). SLBZP treatment effectively downregulated the expression of these pro-inflammatory cytokines at both the transcriptional and translational levels in a dose-dependent manner (Figure 10A–F).

## Effects of SLBZP on Inflammatory Pathways in LPS-Stimulated NCM460 Cells

Western blot analysis showed that phosphorylation levels of p-MAPK p38, p-AKT, and p-NF-κB P65 were elevated in the LPS-stimulated group compared to the control group (Figure 11A). Upon treatment with SLBZP, the expression of these phosphorylated proteins was reduced across all dose groups, with a trend of dose dependence (Figure 11B–D). Total protein levels of MAPK p38, AKT, and NF-κB P65 remained unchanged among groups (Figure 11A).

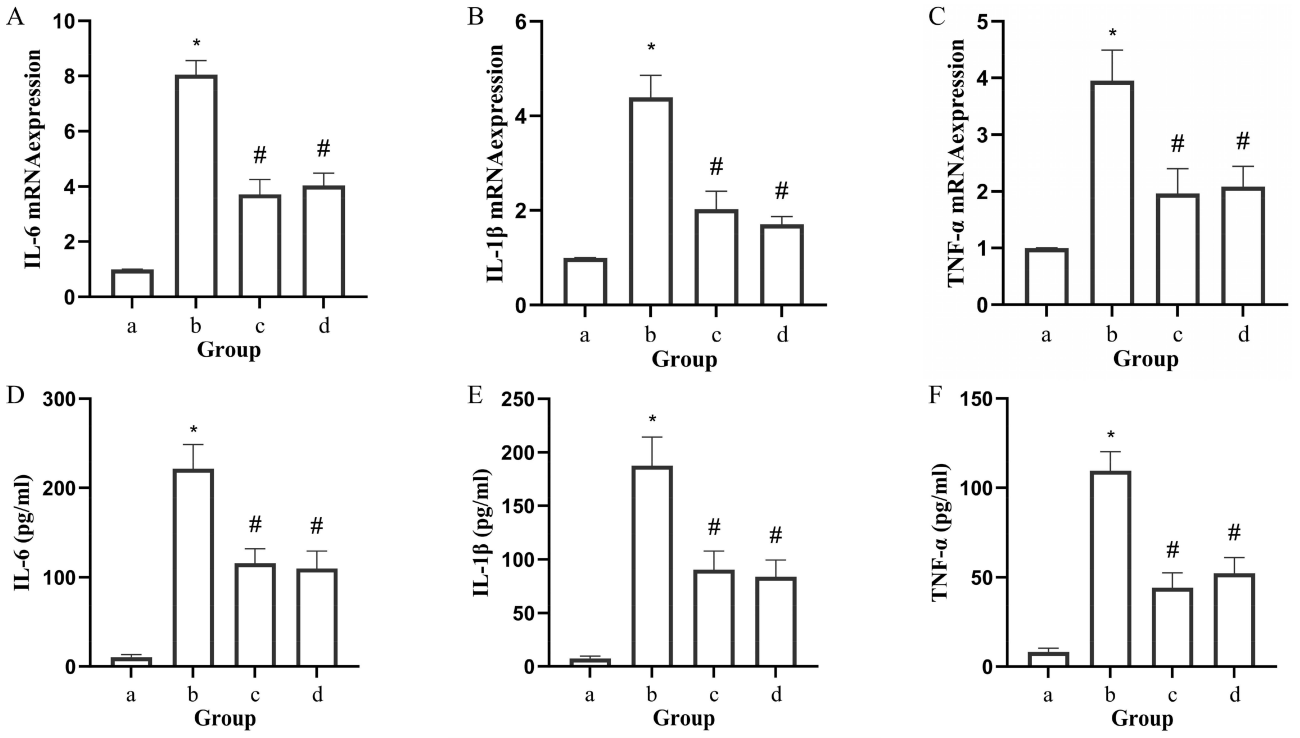


**Figure 7** Cytokine profiling in irinotecan-induced diarrheal model. (**A**) Expression of IL-6 mRNA in jejunal tissue across different rat groups (n=6). (**B**) Expression of IL-1β mRNA in jejunal tissue across different rat groups (n=6). (**C**) Expression of TNF-α mRNA in jejunal tissue across different rat groups (n=6). (**D**) Expression of IL-6 protein expressionin jejunal tissue across different rat groups (n=6). (**E**) Expression of IL-1β protein expression in jejunal tissue across different rat groups (n=6). (**F**) Expression of TNF-α protein expression in jejunal tissue across different rat groups (n=6). a: Blank control group; b: Model group; c: SLBZP group; d: GGQLD group. *p<0.05 vs.Blank control group; #p<0.05 vs Model group.

## Discussion

In traditional Chinese medicine (TCM) theory, the symptoms of irinotecan-induced acute diarrhea resemble those of the "damp-heat diarrhea syndrome", and GGQLD is commonly used for clinical management.[35,36] Previous studies have shown that GGQLD alleviates irinotecan-related diarrhea by suppressing intestinal inflammation and modulating gut microbiota, making it the positive control in this study.[37,38] Conversely, irinotecan-induced delayed diarrhea aligns with the "spleen deficiency with dampness syndrome" in TCM. SLBZP, a classical herbal formula for treating spleen deficiency with dampness, has been applied clinically for managing IAD.[39,40]

However, the mechanism by which SLBZP treats irinotecan-related diarrhea remains unclear. Using public databases, we identified the active components of SLBZP and employed network pharmacology to predict its therapeutic mechanisms. Analysis of the therapeutic targets of SLBZP for IAD through PPI network revealed that the top 20 key targets included IL6, MYC, STAT3, BCL2, TNF, CTNNB1, IL1B, HIF1A, PTGS2, RELA, BCL2L1, CCND1, MMP9, CASP9, PARP1, CXCL8, EGF, MAPK1, ALB, and CASP8. Among these, IL6, TNF, and IL1B are critical pro-inflammatory cytokines involved in inflammatory responses and play pivotal roles particularly in the context of intestinal inflammation.[41] CXCL8 (IL-8), a potent chemokine and inflammatory mediator, is produced by various cells during infections, tissue injury, and immune responses.[42] PTGS2 (COX-2) catalyzes the conversion of arachidonic acid to prostaglandins, thereby mediating inflammatory reactions.[43] During tissue inflammation, the infiltration of inflammatory cells and hypermetabolism lead to excessive oxygen consumption, creating a hypoxic microenvironment that induces the transcription and expression of HIF1A.[44] BCL2L1, CASP9, and CASP8 are closely associated with inflammation-mediated apoptosis, while MMP9 plays a pivotal role in inflammation-driven extracellular matrix degradation.[45,46] Notably, STAT3, RELA, and MAPK1 are key proteins in inflammatory signaling pathways, including the JAK/STAT, NF-κB, and MAPK pathways, respectively. In summary, the therapeutic targets of SLBZP for IAD are strongly linked to inflammatory responses.

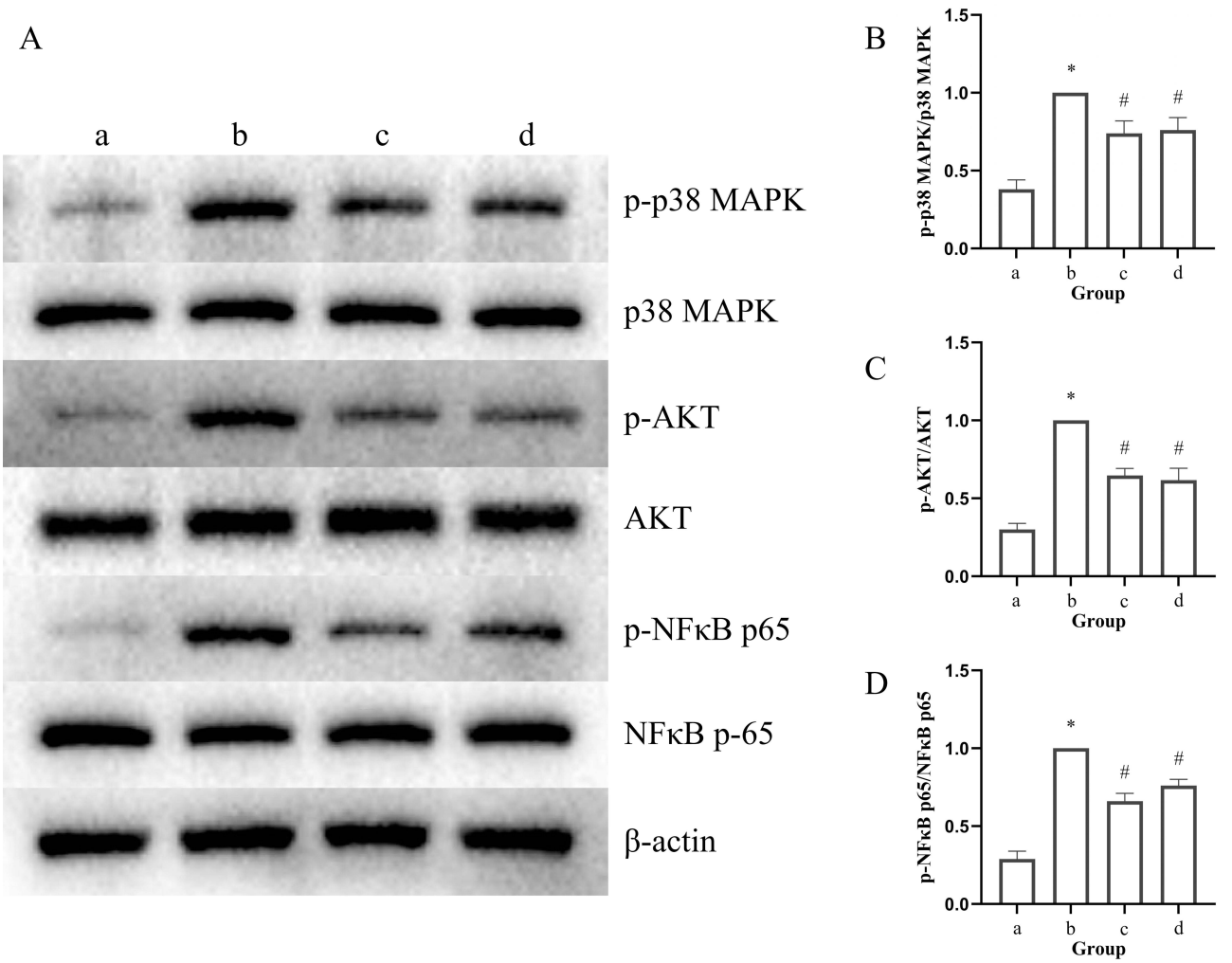


**Figure 8** Western blot analysis of total and phosphorylated protein expression levels of AKT, p38 MAPK, and NF-κB p65. (**A**) Western blot bands. (**B**) The levels of p-p38 MAPK/p38 MAPK (n=6). (**C**)The levels of p-AKT/AKT (n=6). (**D**)The levels of p-NF-κB p65/NF-κB p65 (n=6).a: Blank control group; b: Model group; c: SLBZP group; d: GGQLD group. *p<0.05 vs.Blank control group; #p<0.05 vs Model group.

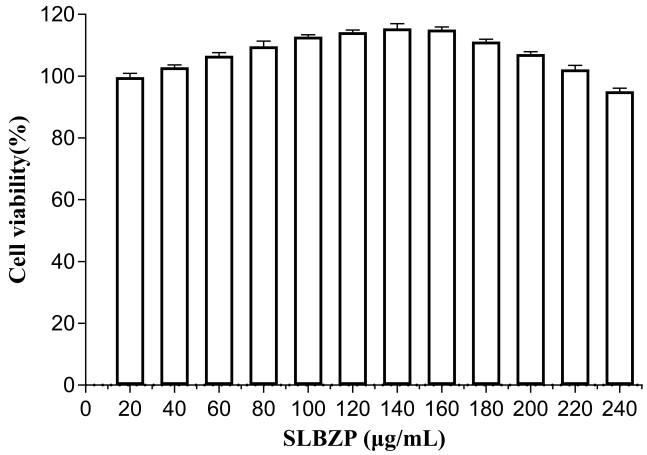


**Figure 9** Effects of different concentrations of SLBZP on the viability of NCM460 cells (n=6).

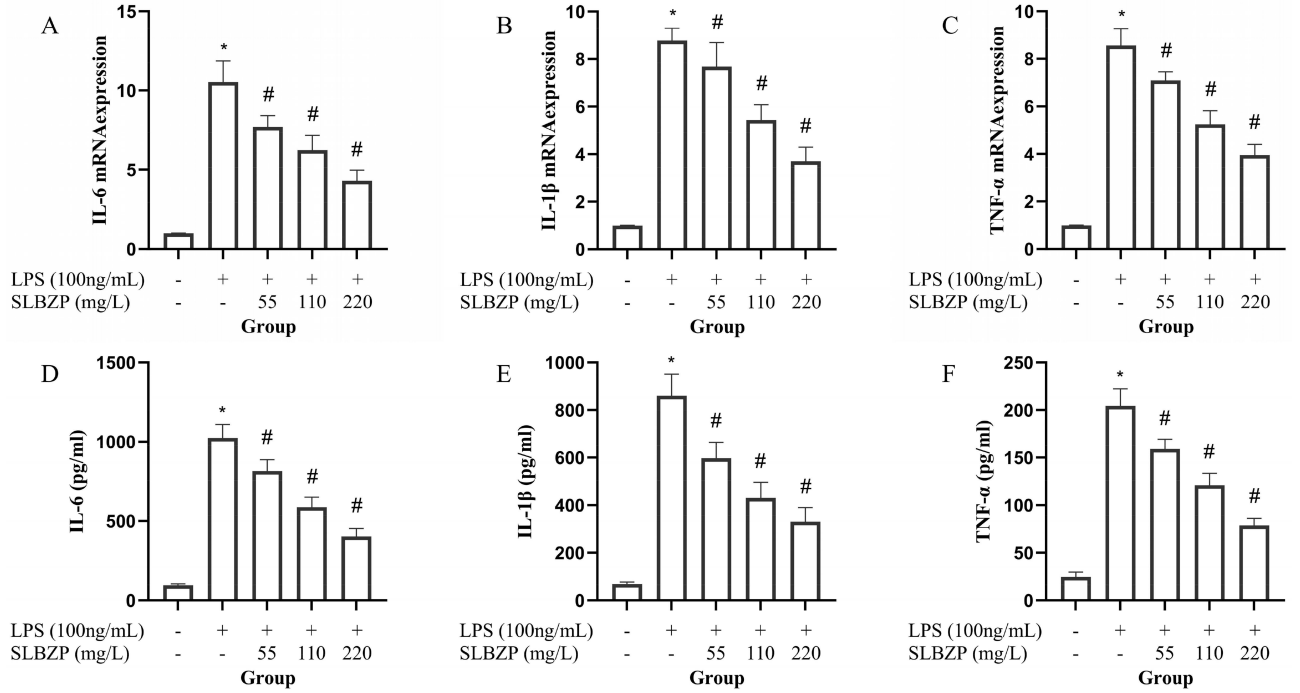


**Figure 10** Effects of SLBZP on pro-inflammatory cytokine expression in LPS-stimulated NCM460 cells. The mRNA expression levels were assessed by qPCR, and their protein concentrations in the culture supernatants were measured by ELISA. (**A**) The levels of IL-6 mRNA (n=6). (**B**) The levels of IL-1β mRNA (n=6). (**C**)The levels of TNF-α mRNA (n=6). (**D**)The levels of IL-6 (n=6). (**E**)The levels of IL-1β (n=6). (**F**) The levels of TNF-α (n=6).*p<0.05 vs.Blank control group; #p<0.05 vs Model group.

In the subsequent KEGG pathway analysis, the top 15 enriched signaling pathways included the PI3K-Akt signaling pathway, MAPK signaling pathway, cellular senescence, IL-17 signaling pathway, apoptosis, HIF-1 signaling pathway, C-type lectin receptor signaling pathway, Th17 cell differentiation, TNF signaling pathway, NOD-like receptor signaling pathway, Toll-like receptor signaling pathway, p53 signaling pathway, NF-κB signaling pathway, FoxO signaling pathway, and apoptosis - multiple species. Among these, the PI3K-Akt signaling pathway, MAPK signaling pathway, Th17 cell differentiation, TNF signaling pathway, NOD-like receptor signaling pathway, Toll-like receptor signaling pathway, and NF-κB signaling pathway are closely associated with inflammatory responses. Previous studies have demonstrated that these inflammatory pathways are critically involved in the pathogenesis of IAD.[47–51] Furthermore, a network interaction map was constructed between these pathways and their corresponding targets, revealing that RELA (NF-κB p65) exhibited the most extensive connectivity with these inflammatory pathways. Meanwhile, the NF-κB signaling pathway transcriptionally regulates key targets predicted by the PPI network, including IL6, TNF, IL1B, HIF1A, PTGS2, MMP9, and CXCL8.[52–54] Based on these findings, we selected the top-ranked PI3K-Akt and MAPK signaling pathways, along with the pivotal NF-κB signaling pathway, for subsequent experimental validation.

The current clinical management of IAD primarily relies on symptomatic antidiarrheal agents, fluid resuscitation, and prophylactic antibiotics.[55–57] While sterile intestinal inflammation is a central pathogenic driver of this condition, glucocorticoids are excluded from therapeutic guidelines due to their detrimental effects. First, glucocorticoids may aggravate intestinal dysmotility via overstimulation of the enteric nervous system, thereby exacerbating diarrheal symptoms. Second, these agents suppress intestinal epithelial cell proliferation, impairing mucosal regeneration and barrier repair. Third, their systemic immunosuppressive properties heighten susceptibility to opportunistic infections by facilitating pathogen translocation. In contrast, SLBZP circumvents glucocorticoid-associated adverse effects. Validating its efficacy in mitigating irinotecan-triggered intestinal inflammatory cascades would therefore provide a clinically impactful therapeutic alternative.

In subsequent studies, we established a rat model of IAD by administering irinotecan via tail vein injection. The model exhibited severe diarrhea, histopathological alterations in jejunal tissue, elevated serum MDA (a pro-oxidative stress marker), and significantly reduced SOD (an antioxidant enzyme) activity. Increased mRNA and protein expression

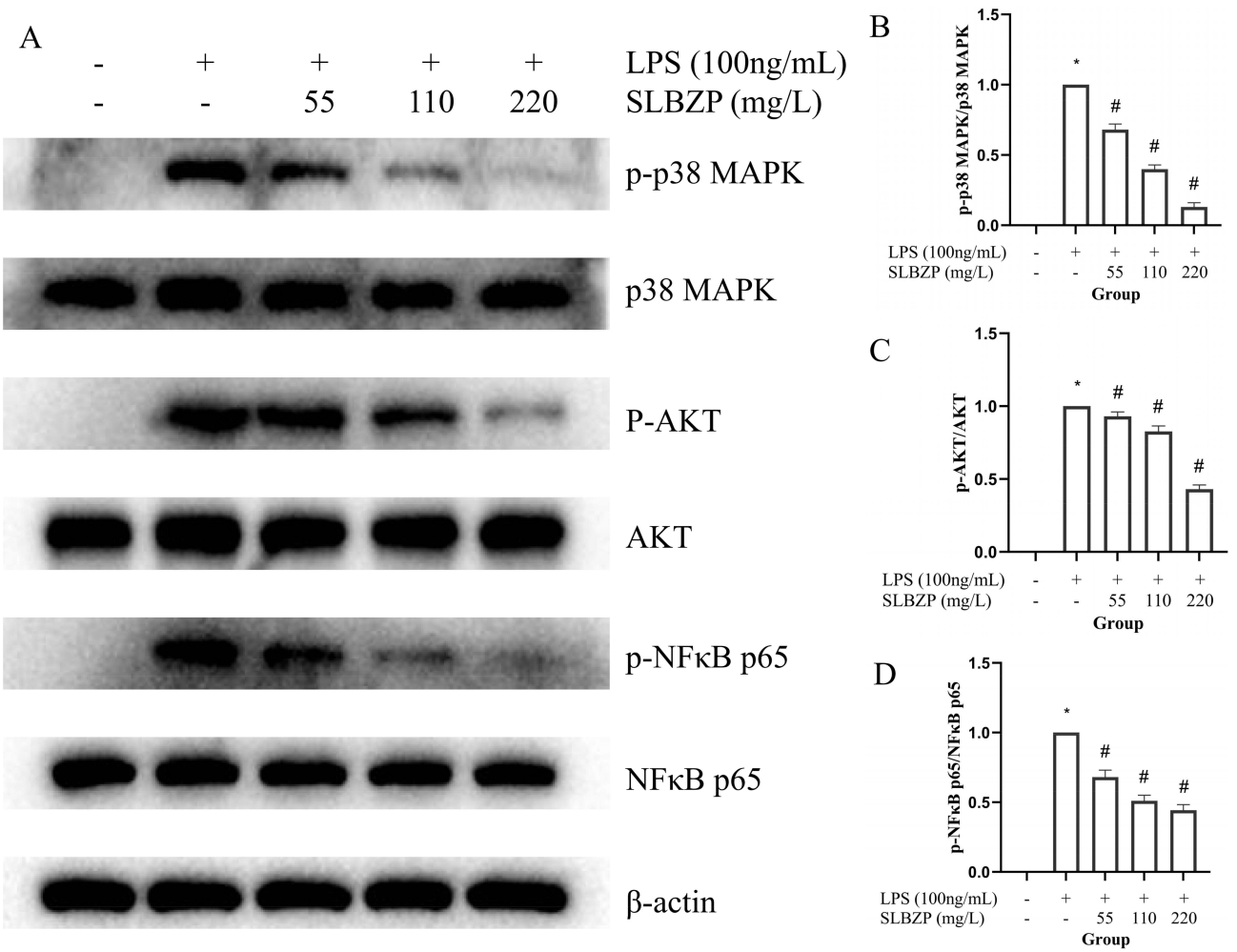


**Figure 11** Western blot analysis of total and phosphorylated protein expression levels of AKT, p38 MAPK, and NF-κB p65. NCM460 cells were stimulated with LPS and treated with SLBZP at low, medium, and high concentrations. Total and phosphorylated levels were detected by Western blot. β-actin was used as a loading control. (**A**) Western blot bands. (**B**) The levels of p-p38 MAPK/p38 MAPK (n=6). (**C**)The levels of p-AKT/AKT (n=6). (**D**)The levels of p-NF-κB p65/NF-κB p65 (n=6). *p<0.05 vs.Blank control group; #p<0.05 vs Model group.

levels of IL-1β, IL-6, and TNF-α, alongside elevated phosphorylation of AKT, MAPK p38, and NF-κB p65, demonstrated aberrant activation of the PI3K/AKT, MAPK, and NF-κB signaling pathways. Intervention with SLBZP markedly alleviated diarrhea severity, ameliorated jejunal histopathological damage, suppressed inflammatory cytokine expression, and attenuated phosphorylation of these signaling proteins. Concurrently, decreased MDA levels and restored SOD activity suggested inhibition of oxidative damage induced by systemic and intestinal inflammation.

We hypothesize that SN-38 induces cell necrosis, releasing inflammatory mediators and exacerbating intestinal damage, while SLBZP mitigates diarrhea by suppressing inflammation. Further in vitro experiments using LPS-stimulated NCM460 cells (human intestinal epithelial cells) demonstrated that SLBZP aqueous extract reversed LPS-induced upregulation of IL-1β, IL-6, and TNF-α mRNA/protein levels and inhibited phosphorylation of AKT, MAPK p38, and NFκB p65, further confirming its anti-inflammatory role.

## Limitations

This study systematically investigated the mechanisms of SLBZP in treating IAD, yet several limitations remain noteworthy. Although SLBZP has been empirically applied for IAD management in clinical practice, its therapeutic efficacy has not been substantiated by randomized controlled trials (RCTs). Future rigorously designed RCTs are imperative to provide evidence-based support for the clinical application of SLBZP. Secondly, the experimental model

utilized in this study only assessed short-term, acute manifestations of IAD. The conclusions of this study are limited by the specific experimental models employed, namely the irinotecan-induced acute diarrhea rat model and the inflammatory response model induced in the NCM460 human colonic epithelial cell line. Currently, there is a lack of widely accepted animal models for irinotecan-induced delayed diarrhea, which restricts further exploration of SLBZP's therapeutic effects on this condition. Although gut microbiota dynamics are recognized as pivotal in IAD pathogenesis, this study primarily focused on integrating network pharmacology with experimental validation to elucidate SLBZP's core mechanisms. Future research will be designed to explore the role of SLBZP in IAD intervention from the perspective of gut microbiota. Lastly, in vitro experiments employed LPS-stimulated NCM460 human colonic epithelial cells to simulate intestinal inflammatory responses. However, the structural complexity of the intestinal tract imposes significant limitations on this model's ability to replicate relevant inflammatory changes. In subsequent studies, we will develop organoid models to better support mechanistic investigations.

## Conclusion

Integrated network pharmacology, in vivo, and in vitro studies demonstrate that SLBZP alleviates IAD primarily by inhibiting aberrant activation of the PI3K/AKT, MAPK, and NFκB pathways and suppressing the expression of inflammatory cytokines IL-1β, IL-6, and TNF-α, providing mechanistic evidence to support its clinical application in managing chemotherapy-induced intestinal toxicity.

## Ethics Statement

In accordance with the Measures for Ethical Review of Life Science and Medical Research Involving Human Subjects (promulgated on February 18, 2023, China), the research involving public data complies with the criteria for ethical exemption. Animal related research were approved by the Animal Ethics Committee of the China-Japan Friendship Hospital (Approval No. ZRYHYY21-22-08-06) and were conducted in strict compliance with the 3R principles (Replacement, Reduction, Refinement) to ensure ethical animal welfare standards.

## Funding

This study was supported by the National High Level Hospital Clinical Research Funding (No. 2022-NHLHCRF-LX-02-0109).

## Disclosure

The authors report no conflicts of interest in this work.

## References

1. Bailly C. Irinotecan: 25 years of cancer treatment. *Pharmacol Res*. 2019;148:104398. Doi:10.1016/j.phrs.2019.104398
2. Mahdy MS, Azmy AF, Dishisha T, et al. Irinotecan-gut microbiota interactions and the capability of probiotics to mitigate Irinotecan-associated toxicity. *BMC Microbiol*. 2023;23(1):53. doi:10.1186/s12866-023-02791-3
3. Yue B, Gao R, Wang Z, Dou W. Microbiota-host-irinotecan axis: a new insight toward irinotecan chemotherapy. *Front Cell Infect Microbiol*. 2021;11:710945. doi:10.3389/fcimb.2021.710945
4. Hulshof EC, Deenen MJ, Nijenhuis M, et al. Dutch pharmacogenetics working group (DPWG) guideline for the gene-drug interaction between UGT1A1 and irinotecan. *Eur J Hum Genet*. 2023;31(9):982–987. doi:10.1038/s41431-022-01243-2
5. Sun M, Zhan H, Long X, et al. Dehydrocostus lactone alleviates irinotecan-induced intestinal mucositis by blocking TLR4/MD2 complex formation. *Phytomedicine*. 2024;128:155371. doi:10.1016/j.phymed.2024.155371
6. Costa DVS, Costa DVS, Sousa CNS, et al. The alpha-lipoic acid improves survival and prevents irinotecan-induced inflammation and intestinal dysmotility in mice. *Pharmaceuticals*. 2020;13(11):361. doi:10.3390/ph13110361
7. Akagi T, Hamano H, Miyamoto H, Takeda T, Zamami Y, Ohyama K. Evaluating the impact of loperamide on irinotecan-induced adverse events: a disproportionality analysis of data from the world health organization pharmacovigilance database (VigiBase). *Eur J Clin Pharmacol*. 2025;81(1):129–137. doi:10.1007/s00228-024-03767-6
8. Tang L, Li X, Wan L, Xiao Y, Zeng X, Ding H. Herbal medicines for irinotecan-induced diarrhea. *Front Pharmacol*. 2019;10:182. doi:10.3389/fphar.2019.00182
9. Zheng Z, Srinual S, Chen J, et al. Herbal medicines as adjuvants for the treatment of chemotherapy-induced diarrhea. *Curr Drug Metab*. 2023;24(6):422–433. doi:10.2174/1389200224666230817102224
10. Deng C, Lou Y, Gao Y, Deng B, Su F, Jia L. Efficacy and safety of Shengjiang Xiexin decoction in prophylaxis of chemotherapy-related diarrhea in small cell lung cancer patients: study protocol for a multicenter randomized controlled trial. *Trials*. 2020;21(1):370. doi:10.1186/s13063-020-04275-5

11. Lu H, Qin J, Han N, Xie F, Gong L, Li C. Banxia xiexin decoction is effective to prevent and control irinotecan-induced delayed diarrhea in recurrent small cell lung cancer. *Integr Cancer Ther*. 2018;17(4):1109–1114. doi:10.1177/1534735418801532
12. Sun R, Basu S, Zeng M, et al. Intervening irinotecan's disposition: the potential of XCHT in alleviating irinotecan-induced diarrhea. *Curr Cancer Drug Targets*. 2019;19(7):551–560. doi:10.2174/1568009618666181029153255
13. Chen J, Shen B, Jiang Z. Traditional Chinese medicine prescription Shenling BaiZhu powder to treat ulcerative colitis: clinical evidence and potential mechanisms. *Front Pharmacol*. 2022;13:978558. doi:10.3389/fphar.2022.978558
14. Cao Y. The mechanism of action of Shen Ling Bai Zhu San and its application in tumor treatment. *Asia-Pacific Trad Med*. 2019;15(04):213–215.
15. Yang Q. Chemotherapy (irinotecan plus raltitrexed) assisted by modified shenling baishu san in the treatment of late colorectal cancer:a clinical study. *Chin J Coloproctol*. 2021;41(02):14–16.
16. Chen GY, Liu XY, Yan XE, et al. Total flavonoids of rhizoma drynariae treat osteoarthritis by inhibiting arachidonic acid metabolites through AMPK/NFκB pathway. *J Inflamm Res*. 2023;16:4123–4140. doi:10.2147/JIR.S418345
17. Chen GY, Wang YF, Yu XB, et al. Network pharmacology-based strategy to investigate the mechanisms of cibotium barometz in treating osteoarthritis. *Evid Based Complement Alternat Med*. 2022;1826299.
18. Chen GY, Liu XY, Luo J, Yu XB, Liu Y, Tao QW. Integrating network pharmacology and experimental validation to explore the key mechanism of gubitong recipe in the treatment of osteoarthritis. *Comput Math Methods Med*. 2022;2022:7858925. doi:10.1155/2022/7858925
19. Chen GY, Liu XY, Chen JQ, et al. Prediction of rhizoma drynariae targets in the treatment of osteoarthritis based on network pharmacology and experimental verification. *Evid Based Comp Alternat Med*. 2021;2021:5233462. doi:10.1155/2021/5233462
20. Jin Q, Li J, Chen GY, et al. Network and experimental pharmacology to decode the action of wendan decoction against generalized anxiety disorder. *Drug Des Devel Ther*. 2022;16:3297–3314. doi:10.2147/DDDT.S367871
21. Ru J, Li P, Wang J, et al. TCMSP: a database of systems pharmacology for drug discovery from herbal medicines. *J Cheminform*. 2014;6(1):13. doi:10.1186/1758-2946-6-13
22. Chen GY, Luo J, Liu Y, Yu XB, Liu XY, Tao QW. Network pharmacology analysis and experimental validation to investigate the mechanism of total flavonoids of rhizoma drynariae in treating rheumatoid arthritis. *Drug Des Devel Ther*. 2022;16:1743–1766. doi:10.2147/DDDT.S354946
23. Chen GY, Ji XY, Li Y, Zheng SS, Jin Q, Tao QW. Mechanisms of total glucosides of paeony in alleviating methotrexate-induced liver injury. *Drug Des Devel Ther*. 2025;19:3407–3423. doi:10.2147/DDDT.S521740
24. Bateman A, Martin M-J, Orchard S, UniProt Consortium. UniProt: the universal protein knowledgebase in 2023. *Nucleic Acids Res*. 2023;51(D1):D523–D531. doi:10.1093/nar/gkac1052
25. Stelzer G, Rosen N, Plaschkes I, et al. The genecards suite: from gene data mining to disease genome sequence analyses. *Curr Protoc Bioinformatics*. 2016;54(1):1.30.1–1.30.33. doi:10.1002/cpbi.5
26. Szklarczyk D, Kirsch R, Koutrouli M, et al. The STRING database in 2023: protein-protein association networks and functional enrichment analyses for any sequenced genome of interest. *Nucleic Acids Res*. 2023;51(D1):D638–D646. doi:10.1093/nar/gkac1000
27. Charan J, Kantharia ND. How to calculate sample size in animal studies? *J Pharmacol Pharmacother*. 2013;4(4):303–306. doi:10.4103/0976-500X.119726
28. Reagan-Shaw S, Nihal M, Ahmad N. Dose translation from animal to human studies revisited. *FASEB J*. 2008;22(3):659–661. doi:10.1096/fj.07-9574LSF
29. Kurita A, Kado S, Kaneda N, Onoue M, Hashimoto S, Yokokura T. Alleviation of side effects induced by irinotecan hydrochloride (CPT-11) in rats by intravenous infusion. *Cancer Chemother Pharmacol*. 2003;52(5):349–360. doi:10.1007/s00280-003-0682-0
30. Fischer AH, Jacobson KA, Rose J, Zeller R. Hematoxylin and eosin staining of tissue and cell sections. *CSH Protoc*. 2008;pdb.prot4986. doi:10.1101/pdb.prot4986
31. Hornbeck PV. Enzyme-linked immunosorbent assays. *Curr Protoc Immunol*. 2015;110(1):2.1.1–2.1.23. doi:10.1002/0471142735.im0201s110
32. Rio DC, M A Jr, Hannon GJ, Nilsen TW. Purification of RNA using TRIzol (TRI reagent). *Cold Spring Harb Protoc*. 2010;2010(6):pdb.prot5439. doi:10.1101/pdb.prot5439
33. Harshitha R, Arunraj DR. Real-time quantitative PCR: a tool for absolute and relative quantification. *Biochem Mol Biol Educ*. 2021;49(5):800–812. doi:10.1002/bmb.21552
34. Hnasko TS, Hnasko RM. The western blot. *Methods Mol Biol*. 2015;1318:87–96.
35. Lu J-Z, Ye D, Ma B-L. Constituents, pharmacokinetics, and pharmacology of Gegen-Qinlian decoction. *Front Pharmacol*. 2021;12:668418. doi:10.3389/fphar.2021.668418
36. Wang D, Bi CR, Jiang HY, et al. Efficacy and Safety of Gegen Qinlian Decoction for Pediatric Diarrhea: a Systematic Review and Meta-Analysis. *Evid Based Complement Alternat Med*. 2022;2022:4887259. doi:10.1155/2022/4887259
37. Chen J, Li M, Chen R, et al. Gegen Qinlian standard decoction alleviated irinotecan-induced diarrhea via PI3K/AKT/NF-κB axis by network pharmacology prediction and experimental validation combination. *Chin Med*. 2023;18(1):46. doi:10.1186/s13020-023-00747-3
38. Wu Y, Cheng Y, Yang Y, et al. Mechanisms of Gegen Qinlian Pill to ameliorate irinotecan-induced diarrhea investigated by the combination of serum pharmacochemistry and network pharmacology. *J Ethnopharmacol*. 2021;276:114200. doi:10.1016/j.jep.2021.114200
39. Lai J, Jiang F, Zhuo X, et al. Effects of Shenling Baizhu powder on pyrotinib-induced diarrhea: analysis of gut microbiota, metabonomics, and network pharmacology. *Chin Med*. 2022;17(1):140. doi:10.1186/s13020-022-00696-3
40. Xiao Y, Zhang K, Zhu SY, et al. Shenling Baizhu Powder () ameliorates Pi (Spleen)-deficiency-induced functional diarrhea in rats. *Chin J Integr Med*. 2021;27(3):206–211. doi:10.1007/s11655-020-3259-4
41. Neurath MF. Strategies for targeting cytokines in inflammatory bowel disease. *Nat Rev Immunol*. 2024;24(8):559–576. doi:10.1038/s41577-024-01008-6
42. Cambier S, Gouwy M, Proost P. The chemokines CXCL8 and CXCL12: molecular and functional properties, role in disease and efforts towards pharmacological intervention. *Cell Mol Immunol*. 2023;20(3):217–251. doi:10.1038/s41423-023-00974-6
43. Szczuko M, Kikut J, Komorniak N, Bilicki J, Celewicz Z, Ziętek M. The role of arachidonic and linoleic acid derivatives in pathological pregnancies and the human reproduction process. *Int J Mol Sci*. 2020;21(24):9628. doi:10.3390/ijms21249628
44. McGettrick AF, O'Neill LAJ. The role of HIF in immunity and Inflammation. *Cell Metab*. 2020;32(4):524–536. doi:10.1016/j.cmet.2020.08.002
45. Yu XB, Chen GY, Zhou L, et al. Chondroprotective effects of gubitong recipe via inhibiting excessive mitophagy of chondrocytes. *Evid Based Complement Alternat Med*. 2022;8922021. doi:10.1155/2022/8922021

46. Chen GY, Chen JQ, Liu XY, et al. Total flavonoids of rhizoma drynariae restore the MMP/TIMP balance in models of osteoarthritis by inhibiting the activation of the NF-κB and PI3K/AKT pathways. *Evid Based Complement Alternat Med*. 2021;2021:6634837. doi:10.1155/2021/6634837
47. Zhang Q, Jiang F, Tao J, et al. Effects of Shu Bu Wenshen Guchang recipe on intestinal injury and the TLR4/NF-κB signaling pathways in mice with irinotecan-induced delayed-type diarrhea. *Transl Cancer Res*. 2022;11(9):3250–3259. doi:10.21037/tcr-22-2145
48. Xiao L, Dou W, Wang Y, Deng H, Xu H, Pan Y. Treatment with S-adenosylmethionine ameliorates irinotecan-induced intestinal barrier dysfunction and intestinal microbial disorder in mice. *Biochem Pharmacol*. 2023;216:115752. doi:10.1016/j.bcp.2023.115752
49. Shu X, Xu R, Xiong P, et al. Exploring the effects and potential mechanisms of hesperidin for the treatment of CPT-11-induced diarrhea: network pharmacology, molecular docking, and experimental validation. *Int J Mol Sci*. 2024;25(17):9309. doi:10.3390/ijms25179309
50. Zhang X, Yang Y, Wen M, et al. Supplementary hesperidin alleviated CPT-11-induced diarrhea by modulating gut microbiota and inhibiting the IL-17 signaling pathway. *J Agric Food Chem*. 2025;73(10):5915–5930. doi:10.1021/acs.jafc.4c09602
51. Li Q, Zhang X, Wang W, et al. CPT-11 activates NLRP3 inflammasome through JNK and NF-κB signalings. *Toxicol Appl Pharmacol*. 2015;289 (2):133–141. doi:10.1016/j.taap.2015.09.025
52. Yu H, Lin L, Zhang Z, Zhang H, Hu H. Targeting NF-κB pathway for the therapy of diseases: mechanism and clinical study. *Signal Transduct Target Ther*. 2020;5(1):209. doi:10.1038/s41392-020-00312-6
53. Guo Q, Jin Y, Chen X, et al. NF-κB in biology and targeted therapy: new insights and translational implications. *Signal Transduct Target Ther*. 2024;9(1):53. doi:10.1038/s41392-024-01757-9
54. Barnabei L, Laplantine E, Mbongo W, Rieux-Laucat F, Weil R. NF-κB: at the borders of autoimmunity and inflammation. *Front Immunol*. 2021;12:716469. doi:10.3389/fimmu.2021.716469
55. He Y, Wu L, Qi X, et al. Efficiency of protective interventions on irinotecan-induced diarrhea: a systematic review and meta-analysis. *Integr Cancer Ther*. 2024;23:15347354241242110. doi:10.1177/15347354241242110
56. Xu S, Lan H, Huang C, Ge X, Zhu J. Mechanisms and emerging strategies for irinotecan-induced diarrhea. *Eur J Pharmacol*. 2024;974:176614. doi:10.1016/j.ejphar.2024.176614
57. Yang X, Chen J, Wang Y, Wu Y, Zhang J. Managing irinotecan-induced diarrhea: a comprehensive review of therapeutic interventions in cancer treatment. *Pharmaceuticals*. 2025;18(3):359. doi:10.3390/ph18030359